PHOTONICS Research

Interference-enhanced optical magnetism in surface high-index resonators: a pathway toward high-performance ultracompact linear and nonlinear meta-optics

Lei Kang,[1,2,†] Huaguang Bao,[1,†] and Douglas H. Werner[1,3]

[1]Department of Electrical Engineering and Center for Nanoscale Science, The Pennsylvania State University, University Park, Pennsylvania 16802, USA
[2]e-mail: lzk12@psu.edu
[3]e-mail: dhw@psu.edu

Received 28 June 2019; revised 6 September 2019; accepted 6 September 2019; posted 11 September 2019 (Doc. ID 371256); published 30 October 2019

Artificial magnetism in optical frequencies is one of the most intriguing phenomena associated with metamaterials. The Mie resonance of high-index resonators provides an alternative approach to achieving optical magnetism with simple structures. Given the generally moderate refractive index exhibited by available materials at optical frequencies, Mie resonances usually suffer from coupling between the multipole modes, and the corresponding response of the Mie metasurfaces can be analyzed based on the concept of "meta-optics." Here, we show that the optical magnetism in high-index resonators can be significantly enhanced by adding a highly reflective back mirror to the system. To highlight the transformative ability of this approach for improving meta-optics in the linear and nonlinear regimes, two proof-of-concept demonstrations are presented. Theoretical modeling reveals that low-pump power ultrafast nonlinear optics can be realized in periodic Si nanodisk arrays backed with a gold film, a system supporting guided resonance modes. Moreover, based on the enhanced magnetism of individual high-index resonators, a pair of silicon cuboids is demonstrated as a magnetic antenna for directional excitation of surface plasmon waves. The interference-enhanced magnetism of high-index resonators provides a disruptive technology for enabling meta-optics comprising ultracompact, high-speed, and power-efficient photonic devices.

https://doi.org/10.1364/PRJ.7.001296

1. INTRODUCTION

Magnetism has rarely been considered in a materials' optical response until the recent emergence of metamaterials, which are artificial media exhibiting optical properties determined by their subwavelength building blocks, i.e., meta-atoms [1,2]. In fact, the magnetic response observed in naturally occurring materials generally vanishes at subterahertz (sub-THz) frequencies. In contrast with the physical mechanism behind magnetism in natural materials, the magnetic response from meta-atoms, e.g., split ring resonators, arises from the rotating current induced in the metallic structures by the magnetic component of the incident electromagnetic fields [3]. This capability to strongly interact with the magnetic component of electromagnetic waves has enabled a variety of phenomena [4–6] and also represents an important step toward negative index media [1,7]. Despite the demonstrated flexibility for tailoring magnetic responses at microwave and THz frequencies [8,9], metamaterials based on metallic structures continue to face two primary challenges regarding magnetism in the optical regime: the Ohmic loss due to the scattering of electrons at metal surfaces and the complex process of fabricating meta-atoms with subwavelength features.

Mie resonances of high-index resonators provide an alternative route to achieving strong electric and magnetic responses. In contrast with that in metallic structures, the Mie resonance-based magnetic response originates from the magnetic-field-induced circular displacement current in dielectric resonators [10,11]. High-index resonators have attracted considerable attention for their use as simple building blocks or artificial atoms in the construction of metamaterials. Nevertheless, the extension of Mie resonance based 3D metamaterials into the optical regime has rarely been reported, partially as a result of the difficulty in fabrication. Distinct from metamaterials possessing bulk effective material parameters, optical metasurfaces derive their properties from either a single layer or a few layers of meta-atoms [12,13]. Besides boosting the

performance of planar plasmonic metadevices [14], the metasurface concept has recently been applied to dielectric nanostructures, revealing a variety of interesting phenomena in both the linear and nonlinear regimes. Compared with plasmonic nanostructures, dielectric meta-atoms are more attractive owing to their potential for manipulating optical waves with extremely low losses. It is important to note that, due to the fact that the refractive index of constituent materials at optical frequencies is generally low to moderate, typical dielectric meta-atoms are not considerably smaller than the operating wavelength. As a result, the response of dielectric metasurfaces can be analyzed by employing the concept of "meta-optics" rather than by effective material parameter models. Two review papers have provided a comprehensive description of the recent advances in this fast-developing field [15,16].

The fundamental properties of magnetic Mie resonances are primarily determined by the refractive index of the resonators. In optics, the refractive index of dielectric materials is, in general, moderate, which accordingly gives rise to a variety of unique characteristics that are associated with optical Mie resonances. For instance, the coherent effect, which is defined as the coupling between multipole modes of a dielectric resonator's scattering field, is obvious for Si nanostructures. Therefore, the scattering of optical dielectric resonators generally exhibits typical features of low-quality-factor (Q-factor) spectra and a reduction in the frequency separation between the magnetic and electric resonances [17–20]. Furthermore, the relatively weak confinement of the fields leads to strong interaction between neighboring dielectric meta-atoms, which makes the design of meta-optics even more challenging. The relatively poor field confinement also seriously restricts and impedes the applications of dielectric resonators in the nonlinear regime due to the limited local field enhancement factors. Therefore, a new strategy that would allow enhanced Mie resonance for sharper spectral features in the optical response as well as larger field enhancement is highly desired for meta-optics-based systems operating in the linear and nonlinear regimes.

The interference of coherent waves has been widely exploited in the design of high-Q-factor systems [21], such as in conventional lasers, Fabry–Perot etalons, and micro-ring resonators. On the other hand, by exploiting an index guiding effect that confines light in the third (vertical) dimension [22], guided modes in photonic crystal slabs have been utilized to realize devices in a planar configuration [23,24]. Although the in-plane periodic structure incorporated into such designs provides the phase-matching mechanism, the coupling between the guided modes and surface-normal incident light is primarily constrained by the low refractive index of the optical materials. More recently, Piper and Fan theoretically verified that critical coupling of normally incident light with guided resonances of a photonic crystal slab can be achieved by simply adding a highly reflective mirror that backs the slab [25]. We emphasize that the interference under the critical coupling condition leads to strong mode selection, which can potentially result in a high-Q Mie resonance in dielectric resonators with strong field confinement. In fact, a metallic backplane in these critically coupled systems can facilitate interference and simultaneously provide a loss mechanism. It should be noted that metallic backplanes have been widely adopted in planar metadevices not only for enhancing the optical responses [26,27] but also for enabling multiple functionalities by exploiting other intrinsic properties of metals [28,29]. A metallic substrate has also been used to control the scattering properties of isolated dielectric nanoparticles [30,31].

In this work, by presenting two proof-of-concept studies, we demonstrate that meta-optical systems based on the interference-enhanced magnetism in silicon resonators can potentially serve as a transformative platform for strong linear and nonlinear light–matter interactions. Starting from a study of Mie resonances of Si nanodisks on top of a gold substrate as a function of the resonator array size, the origin of the interference-enhanced optical magnetism in the high-index resonators is revealed. A theoretical analysis of optical nonlinearity suggests that ultrafast all-optical tuning of a Si metasurface backed by a gold film can be realized with pump power an order of magnitude lower than that previously used in the similar systems without backing mirrors. Moreover, by comprehensively using the plasmonic property of the gold ground plane, we demonstrate that a pair of Si cuboids with well-tailored geometries can enable directional excitation of surface plasmon (SP) waves in such meta-optical systems. It should be noted that a recent work reported a broadband giant refractive index (>26) at visible frequencies [32], indicating the promising potential of meta-optical systems toward realizing Mie-resonance-based light manipulation. Our study is motivated by the previously reported all-dielectric optical metasurfaces whose responses are limited by the moderate refractive index of dielectric materials; accordingly, the systems proposed here are distinct from the recently demonstrated metamaterial mirrors [33–35].

2. META-OPTICS BASED ON Si RESONATORS ON A PLASMONIC SUBSTRATE

Critical coupling may allow photonic crystal systems to absorb all incident power and exhibit a vanished reflection coefficient, corresponding to the so-called perfect absorber phenomenon. In previous studies, dielectric Bragg mirrors were proposed to enable the coherent cancellation of the guided resonance, and a lossy but highly transparent thin film (e.g., graphene) was employed to control the intrinsic loss rate of the system [25]. In fact, noble metals in the form of an optically thick film are promising candidates for the requisite substrate that can simultaneously support high reflection and a loss mechanism. Figure 1(a) presents a schematic of the unit cell of the proposed critical coupling metasurface, i.e., a periodic Si nanodisk array backed by an Au substrate. Hydrogenated amorphous silicon (a-Si:H) was adopted because of its remarkably large nonlinearity and ultrafast carrier dynamics. It should be noted that perfect absorbers based on ceramic particles [36] and hyperbolic structures [37] on metallic substrates were previously reported at microwave and mid-IR frequencies, respectively. We emphasize that the proposed metasurfaces display two distinct features from these reported systems. First, Si has extremely low loss at infrared wavelengths, which allows for high-Q-factor guided resonances, while the intrinsic loss rate of the system is primarily determined by the plasmonic substrate. Second,

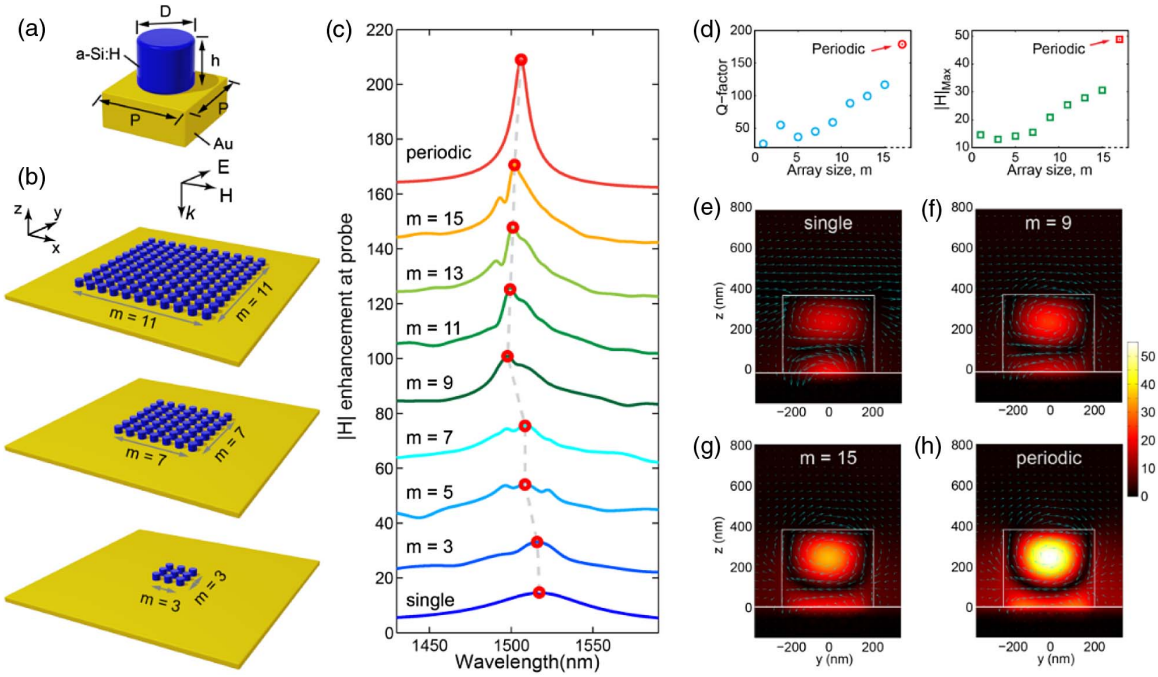

Fig. 1. Meta-optics based on Si resonators on a plasmonic substrate. (a) Illustration of a unit cell of the metasurface consisting of an array of a-Si:H nanodisks on top of an optically thick Au ground plane. Geometrical parameters: $P = 720$ nm, $D = 450$ nm, and $h = 385$ nm. (b) Schematic of the proposed meta-optical systems with finite array size, in which square arrays having $m \times m$ a-Si:H nanodisk elements are located on top of an infinite Au substrate. (c) Calculated magnetic field ($|H|$) obtained from a magnetic probe located at the center of the central resonator for a series of array sizes used in numerical simulations. The gray dashed line is used to guide the eye. (d) Q-factor and the maximum enhancement factor $|H|_{\max}$ as functions of the array size. The corresponding values in the periodic case are illustrated as well. (e)–(h) Calculated magnetic field and electric field vector distribution in the y–z plane, in the case of $m = 1$, 9, and 15 as well as the periodic structure at the peak frequency identified in (c).

the plasmonic property of the Au substrate not only assists the critical coupling at the dielectric/metal interface but also offers a unique opportunity to couple free-space radiation to surface plasmon polaritons (SPPs). Jointly, these characteristics differentiate our system from all previously reported meta-optical systems [38,39] that involve no surface plasmon effects.

Given the coexistence of Mie resonances and SPPs, it is important to investigate the influence of structural factors on the guided resonance properties. On the other hand, Si metasurfaces are known to exhibit array size-dependent responses [40]. Consequently, as illustrated in Fig. 1(b), we numerically examine the resonant properties of the proposed metasurfaces as a function of the array dimensions. The metasurfaces are illuminated by a linearly polarized plane wave propagating along the $-z$ direction, and, to quantitatively evaluate the Mie resonance, a magnetic field probe is placed at the center of the central element of each nanodisk array. Figure 1(c) shows the magnitude of the magnetic field ($|H|$) obtained at the probe, normalized to that of the incident field, for a series of metasurface array sizes (values of m). That of a periodic structure [Fig. 1(a)] is also included for comparison purposes. With an increasing resonator array size, Fig. 1(c) suggests a clear evolution of the magnetic resonance-based coupling between incident light and the Si resonators. The corresponding extracted Q-factors and the maximum field enhancement factor ($|H|_{\max}$) as functions of m are shown in Fig. 1(d), in which an unambiguous increasing trend can be identified. In particular, the Q-factor and the $|H|_{\max}$ reach ~180 and ~49, respectively, for a periodic structure, compared with the corresponding values of ~26 and ~14 when the system contains only a single Si nanodisk ($m = 1$). On the other hand, as indicated by the dispersion of $|H|$ [Fig. 1(c)], the Mie resonance of the nanodisks only experiences a slight frequency change with varying values of m [see gray dashed line in Fig. 1(c)], indicating that the observed coupling is primarily determined by the intrinsic properties of the meta-optical system. The slight change in the resonance frequency is attributed to the discontinuity at the edges of the array, while, as the array size increases, the response of the finite structure converges toward that of the periodic structure. Figures 1(e)–1(h) depict the normalized magnetic field distribution and electric field vectors on a plane cutting through the central element of each nanodisk array, for the cases of $m = 1$, 9, and 15 as well as a periodic structure. A displacement current loop indicated by the circulating electric field vectors and the significantly enhanced magnetic field on the upper side of the resonator can be clearly observed in each plot. In particular, the field distribution profile that is less contingent on the array size further reveals the intrinsic resonant characteristics of the proposed metasurface. It is also obvious that stronger field confinement and enhancement can be achieved as the size of the nanodisk array increases. We note that the field enhancement observed in Fig. 1(h) is approximately one order of magnitude stronger than that identified in metasurfaces based on Si resonators on top of a dielectric

(e.g., glass) substrate. These unique properties may allow the proposed system to enable a variety of functionalities based on the concept of meta-optics. To highlight the novel role of interference-enhanced magnetism in reshaping meta-optics, hereinafter we present two proof-of-concept demonstrations.

3. ULTRAFAST NANOPHOTONICS ENABLED BY GUIDED MAGNETIC MIE RESONANCES

Developing nanophotonic systems that can be tuned in an active manner is an intriguing direction for research and development of optical devices. Among the variety of different types of active nanophotonic devices, optical modulators have attracted a considerable amount of attention due to their importance in nano-optics. However, the performance of conventional modulators, either the absorptive type or refractive type, is limited by the moderate optical property change in the active materials. Consequently, two primary strategies have been successfully employed to maximize the tunability: (1) accumulating the tuning by allowing longer propagation lengths of light in extended structures, such as optical waveguides, and (2) creating high Q-factor resonating structures, such as micro-ring resonators, to increase the modulation sensitivity but at the expense of an increase in the overall footprint of the systems.

Recent studies have presented approaches to exploit the opportunities that dielectric metasurfaces offer for nonlinear nanophotonics arising from the nonlinear dynamic processes in dielectric meta-atoms [39,41–43]. By exploiting the Mie-resonance-enhanced two-photon absorption (TPA), Shcherbakov *et al.* have demonstrated a 65 fs transmission switching with a modulation depth of 1% at visible frequencies in Si nanodisk arrays by performing pump–probe experiments [39]. Employing the second primary strategy discussed above, Yang *et al.* created high Q-factor resonances in a Fano-resonant metasurface that exhibit a sharp linear transmittance spectrum and have demonstrated a transmission modulation depth up to 36% [41]. To enable the "bright" and "dark" modes as well as their coupling, each unit cell in this study includes a bar resonator and a disk resonator, inevitably resulting in a reduced design flexibility.

On the other hand, numerical simulations implementing periodic boundary conditions can provide an effective means for analyzing the linear response and optical nonlinearities of Si metasurfaces. Recently, Della Valle *et al.* developed a theoretical model that can describe the dynamic processes in a-Si:H metasurfaces by accurately reproducing all the features observed in the pump–probe experiments [38]. Importantly, by fully considering the three mechanisms that dominate the nonlinear dynamics of a-Si:H nanostructures (i.e., instantaneous TPA, free-carrier generation and relaxation, and lattice heating) and coupling them together by a system of rate equations, this theoretical model can accurately describe the transient permittivity change $\Delta\varepsilon$ of Si. Then, using this dynamic transient permittivity, the authors showed that the transient optical response (transmission/reflection, etc.) can be calculated as a perturbation of linear numerical simulations. The TPA leads to a purely imaginary instantaneous change in the permittivity, while the free-carrier generation due to linear or nonlinear absorption processes results in a transient Drude plasma permittivity, and the lattice heating effect induces a thermo-optical modulation. This model provides a powerful tool for understanding and quantitatively predicting the ultrafast modulations of Si metadevices based on all-optical excitations. Here, by employing full-wave simulations and using the model presented in Ref. [38], we investigate the linear and nonlinear responses of the proposed meta-optical systems. In our modeling, we have adopted the measured amorphous silicon property reported in Ref. [39] and the corresponding nonlinear coefficients used in Ref. [38].

As the schematic in Fig. 2(a) shows, a plane wave at normal incidence is used as the probe light, and laser pulses at 800 nm, with a pulse duration of 100 fs, are applied as the excitation source for the nonlinear dynamics analyses presented herein. The simulated linear reflectance (R) [absorption ($A = 1 - R$, since $T = 0$)] spectrum is shown in the inset of Fig. 2(b),

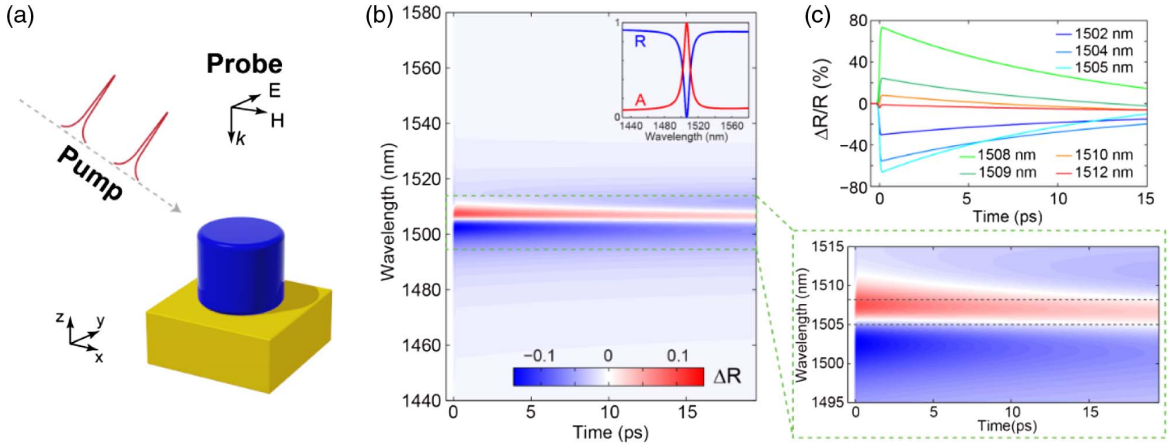

Fig. 2. All-optical ultrafast modulation enabled by critical coupling with the guided resonance of meta-optical systems. (a) Schematic of the unit cell used in numerical simulations. The geometrical parameters are the same as those used in Fig. 1(a). The ultrafast nonlinear responses of the proposed metasurface are obtained by implementing the theoretical model presented in Ref. [38]. (b) Transient absolute reflectance modulation (ΔR) under pumping at an 800 nm wavelength with a pump fluence of 0.1 mJ/cm^2. The pump intensity is 10% of that used in Ref. [38]. For clarity, the results around the resonance are enlarged and shown on the right (dashed-green box). The simulated static reflectance and absorption spectra are shown in the inset. (c) Relative differential reflectance ($\Delta R/R$) at a few wavelengths of interest near the resonance.

in which a sharp dip with minimum R of ~0 is identified around a wavelength of 1500 nm. Originating from the critical coupling with a guided resonance of the Si metasurface, these resonance characteristics in the linear regime imply the existence of an in-depth all-optical modulation at low pump intensity. Consequently, assuming a pump fluence $F = 0.1\ \mathrm{mJ/cm^2}$, which is 10% of that used in Ref. [38], we numerically investigate the nonlinear dynamics of the proposed meta-optical system. The simulated reflectance modulation (ΔR) as a function of probe wavelength and time delay between the pump and probe pulses is shown in Fig. 2(b). A maximum ΔR of −0.1 and 0.1 is, respectively, identified on the two sides of the resonance around 1505 nm, which can be more clearly seen in the enlarged plot shown on the right. Moreover, in Fig. 2(c), we show the transient traces of the differential reflectance ($\Delta R/R$) at a few wavelengths of interest near the resonance. A positive (negative) transient modulation with maximum modulation depth >70% (>−60%) is identified at the longer-wavelength (shorter-wavelength) side of the resonance. In addition, these observed transient responses reveal a rise time of ~100 fs and a decay time constant of ~15 ps. It has been shown that the former is determined by the pump pulse's duration, while the latter primarily depends on the carrier relaxation process in a-Si:H and its complicated interaction with the lattice heating effect [38,39]. Arising from the critical coupling-enabled near-zero reflectance, a $\Delta R/R$ as high as 500% was also found at the resonance wavelength (not shown), with a concomitant significant increase in decay time, which is, however, undesired for applications based on ultrafast optics. It should be noted that, because of the low optical excitation fluence assumed in our studies, the changes in optical properties of the Si resonator are rather moderate, indicating the excellent ultrafast modulation sensitivity of the proposed meta-optical systems.

Given the fact that Mie-resonance-based metasurfaces exhibit great flexibility in tailoring their resonance properties by varying the dielectric resonator geometries, it is straightforward to extend the ultrafast modulation behavior shown in Fig. 2 to systems with more complicated responses in the linear regime for sophisticated nonlinearity. For instance, simply changing the geometrical symmetry of the resonators may enable polarization-dependent and/or multiband linear and nonlinear responses. As the schematic in Fig. 3(a) shows, we consider a metasurface consisting of an array of Si nanodisks with an elliptical cross-section on top of an Au backplane. The inset of Fig. 3(b) shows that the long axis of the nanodisks is aligned along $\alpha = 45°$. As shown in Fig. 3(b), for a y-polarized normally incident wave, two dips are identified in the linear co-polarized (R_{yy}) reflectance spectrum at wavelengths around 1530 and 1550 nm. Furthermore, due to the cross-polarization coupling effect originating from the geometrical anisotropy of the nanodisks, two peaks are seen to be present in the R_{xy} reflectance spectrum. The dynamics of the cross-polarized component, which may lead to distinct transient characteristics, can be exploited to enrich the variety of nonlinear phenomena that can be observed in the proposed metasurfaces. To confirm the origin of the two resonance modes, distributions of the magnetic field and its vector plots cutting through the middle of the Si nanodisk are shown in Fig. 2(b). Two resonances that clearly originate from the geometric anisotropy of the structure are identified along with field enhancement factors that are as large as 30 times.

By assuming the same pump fluence used to generate the results shown in Fig. 2, we investigate the nonlinear dynamics of this elliptical Si nanodisk based metasurface for both the co- and cross-polarized field components. Figure 3(c) illustrates the simulated reflectance modulation for the co-polarized component ΔR_{yy}. Two obvious wavelength regions with considerable modulation in absolute reflectance are observed. As shown in Fig. 3(d), a positive ultrafast modulation with a maximum modulation depth greater than 6% and 5% is identified at 1531 and 1558 nm, respectively, while a negative transient modulation greater than −6% is found at 1526 and 1550 nm. As shown in Fig. 3(e), remarkably large modulation can be achieved at wavelengths (e.g., 1528 and 1554 nm) closer to the linear resonances. Despite the long recovery time, indicated by a long-duration plateau [Fig. 3(e)], the observed ultrafast dynamics indicate a transient modulation in the sub-picosecond regime, which can be attributed to the instantaneous TPA process [38]. These observations agree well with the experiments shown in Ref. [39]. Figure 3(f) depicts the nonlinear dynamics of ΔR_{xy}, in which two bands with negative absolute modulation as large as −0.05 are seen. This negative modulation ($\Delta R_{xy} < 0$) results from the permittivity change of Si under low-power excitation. Figure 3(g) further illustrates the transient traces at a few wavelengths around the two resonance modes. A comparison with Fig. 2(b) shows that the nonlinear characteristics of the elliptical Si nanodisk metasurfaces, including the dual-band response and polarization sensitivity, are particularly attractive for power-efficient ultrafast nanophotonics.

4. MAGNETIC MIE RESONANCE BASED DIRECTIONAL EXCITATION OF SURFACE PLASMON WAVES

SP waves are, in general, referred to as electromagnetic waves propagating along a metal-dielectric interface. Due to their unique characteristics, including subwavelength confinement and field enhancement, SPPs show great potential for applications in various photonic devices, such as all-optical integrated circuits and chemo- and bio-sensors. Due to the momentum mismatching between the free-space photons and SPPs, a variety of approaches have been utilized to provide the necessary momentum conservation required for SPP excitation. Given the rather limited propagation length of SP waves due to the loss of metals, efficient schemes for the excitation of SPPs are of critical importance in nano-optics. It has been demonstrated that the directional excitation of SPPs can potentially enable controllable scattering, interference, and localization of SPPs for numerous applications associated with 2D optics, providing more degrees of freedom for the design and exploitation of plasmonic devices.

To overcome the disadvantages of conventional couplers such as their large footprints, SPP couplers based on nanostructures on a metal surface have been studied intensively [44–47]. In particular, to excite directional SPP waves, two primary strategies have been employed: (1) illuminating the symmetric

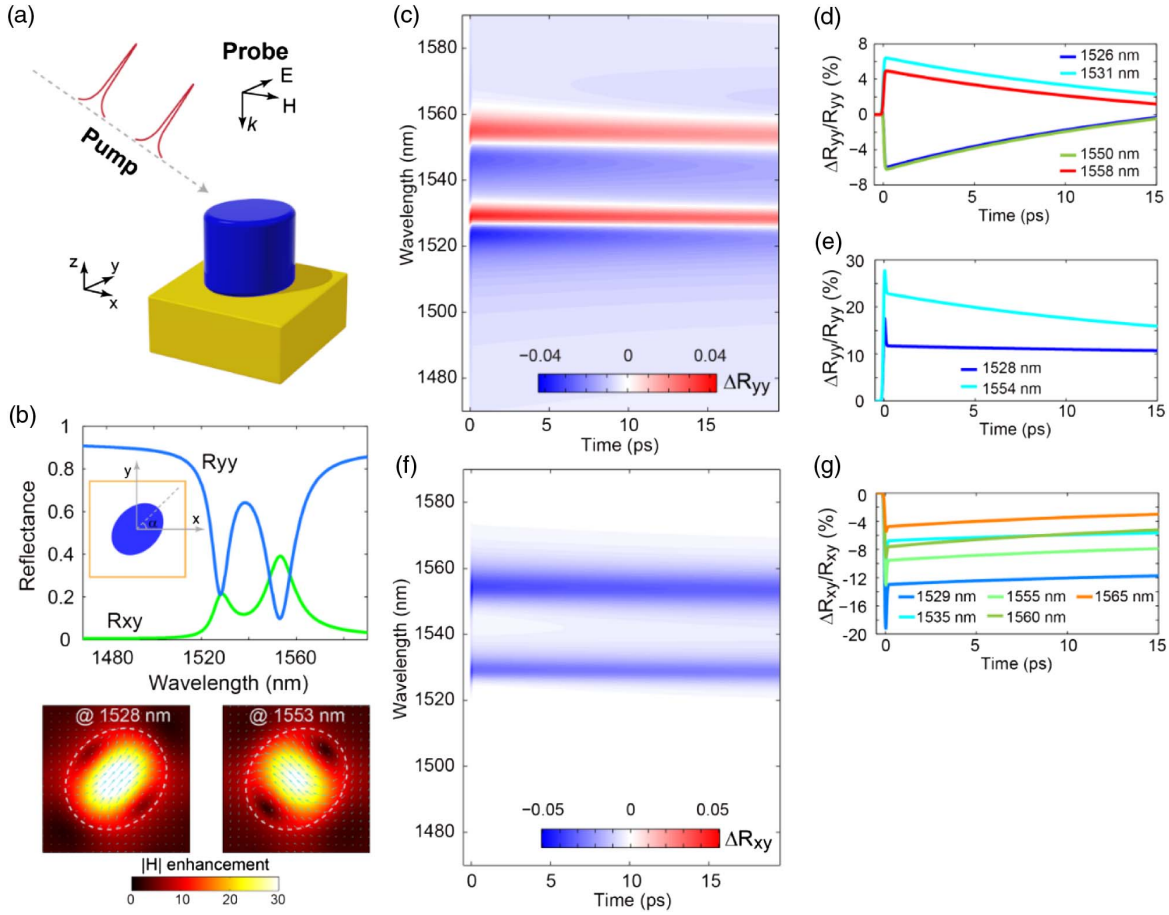

Fig. 3. Polarization sensitive ultrafast modulation based on Si nanodisks with an elliptical cross-section. (a) Schematic of the unit cell used in numerical simulations. The major and minor axes of the elliptical cross-section are 500 and 450 nm, respectively. (b) The cross- and co-polarization reflectance spectra when the metasurface is illuminated by a *y*-polarized wave. Inset indicates the orientation of the Si nanodisk in the *x*–*y* plane. Calculated magnetic field (normalized to that of the incident wave) and its vector distribution in a plane cut across the middle of the resonator at the two resonance wavelengths (bottom). Transient absolute reflectance modulation for (c) the co-polarization reflected wave (ΔR_{yy}) and (f) the cross-polarization reflected wave (ΔR_{xy}) under pumping at an 800 nm wavelength with a pump fluence of 0.1 mJ/cm^2. Relative differential reflectance (d), (e) ($\Delta R_{yy}/R_{yy}$) and (g) ($\Delta R_{xy}/R_{xy}$) at a few wavelengths of interest.

nanostructures (e.g., nanowires and nanoslits) with obliquely incident light, and (2) creating in-plane asymmetric nanostructures. Although for both strategies the directional excitation can be attributed to the symmetry breaking of the excitation systems, the latter is more attractive due to its capability of coupling normally incident light to SPPs. As an alternative to the nanostructure-based scattering-enabled momentum matching, Liu *et al.* demonstrated efficient directional SPP generation based on a pair of plasmonic magnetic antennas [48]. However, the plasmonic property of the metallic nanoantennas inevitably causes high Ohmic loss at the resonance wavelengths.

Figures 1(c) and 1(e) show that a strong magnetic resonance can be achieved within an isolated Si resonator located on top of a gold substrate, indicating the potential use of high-index resonators for enabling ultracompact SPP couplers. As the schematic in Fig. 4(a) illustrates, we first study a system with an individual cuboid-shaped Si resonator on top of an optically thick gold substrate. The presence of the gold substrate not only facilitates the enhanced optical magnetism in the high-index resonator but also simultaneously provides the metal–dielectric interface that supports the propagation of SPPs. Besides its ability to improve the SPP excitation efficiency, the cuboid resonator was adopted to simultaneously enable polarization selectivity under normal incidence conditions. For the system illustrated in Fig. 4(a), symmetric bi-directional SPP generation is expected. To analyze the correlation between the magnetic resonance of the cuboid and the SPP excitation, a magnetic field (*H*-field) probe is placed in the geometric center of the cuboid, while an electric field (*E*-field) probe is set to be 5 μm away from the resonator (10 nm above the gold substrate) to monitor the generated SPPs. It should be noted that the use of an *E*-field probe that is far enough from the resonator allows for the detection of the *z*-component of the electric field (E_z) resulting from the excited SPP, excluding both the scattering effect in the near field of the resonator and the field associated with the (*y*-polarized) incident wave.

Figures 4(b) and 4(c) depict E_z and H_x at the *E*-field and *H*-field probes, respectively, when a cuboid resonator of distinct lateral dimensions (Cuboid A and Cuboid B) is excited by a plane wave of magnitude $E_0 = 1$ V/m. The same height

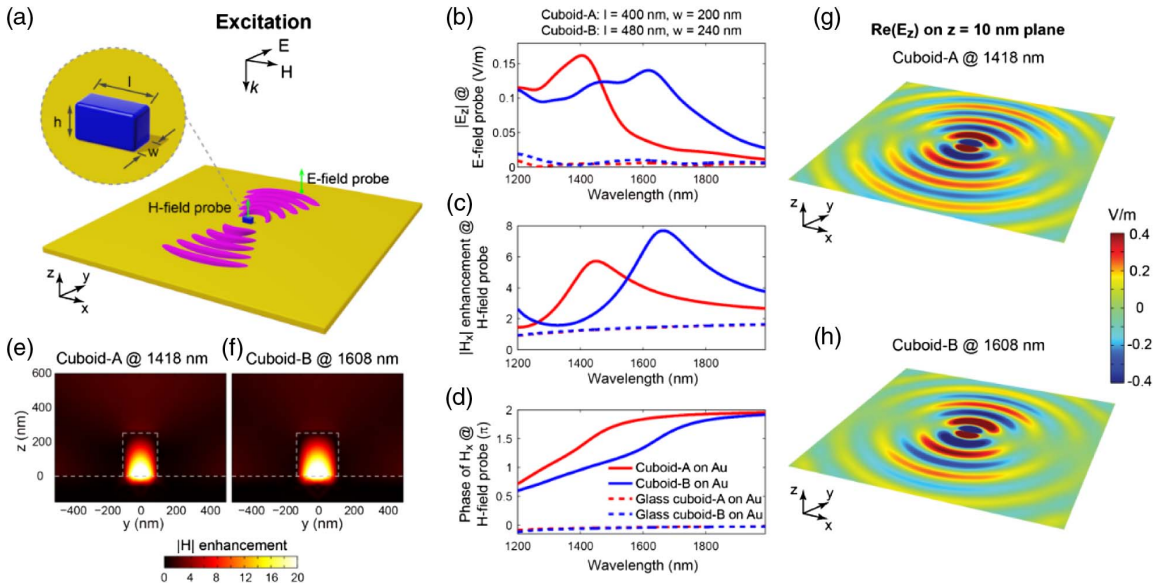

Fig. 4. Exploiting the magnetic response in individual high-index resonators for excitation of SPPs. (a) Schematic of the meta-optical system that includes a Si cuboid located on a gold substrate. Around the magnetic Mie resonance of the resonator, SPPs primarily propagating along the $+y$ and $-y$ directions will be excited on the surface of the gold substrate. A y-polarized plane wave normally illuminates the resonator from the top. A magnetic (H) field probe is placed in the center of the cuboid, and an electric field probe is placed 10 nm above the gold surface at $y = 5$ μm. (b) Magnitude of E_z detected at the E-field probe and (c) magnitude and (d) phase of H_x detected at the H-field probe, when the SP wave is excited by a Si cuboid of two distinct geometries (Cuboid A: $l = 400$ nm, $w = 200$ nm; Cuboid B: $l = 480$ nm, $w = 240$ nm). For comparison purposes, the results based on a glass cuboid of the same dimensions are shown in (b)–(d) as well (dashed curves). (e), (f) The magnetic field distribution for both excitation systems at a wavelength where $|E_z|$ peaks. The electric field distribution of SPPs excited on the gold surface (g) by Cuboid A and (h) by Cuboid B.

[$h = 280$ nm in the inset of Fig. 4(a)] was assigned to both cuboids to ensure that the designs can be fabricated. For either resonator, the dispersions of both E_z [Fig. 4(b)] and $|H_x|$ [Fig. 4(c)] peak at the same wavelength (i.e., ∼1400 nm for Cuboid A and ∼1600 nm for Cuboid B), which unambiguously indicates the correlation between the Mie magnetic resonance and the SPP excitation in the system. Given the fact that the relative phase difference between two couplers primarily determines the potential directional excitation of SPP, it is of more interest to examine the phase information of the Mie resonance obtained at the H-field probe [Fig. 4(d)]. A continuous phase difference with a maximum value greater than $\pi/2$ is identified in the wavelength range of interest, revealing the potential of the proposed meta-optical system with two Si cuboids for directional SPP excitations. For comparison purposes, results of the system with an isolated glass ($n = 1.5$) cuboid of the same dimensions on a gold substrate are also shown as the dashed curves in Figs. 4(b)–4(d). Only rather weak SPPs can be excited; more importantly, adjustment of the glass cuboids' dimensions makes almost no difference in the excitation behavior of the system [Figs. 4(c) and 4(d)]. This results from the fact that the examined glass cuboids cannot support magnetic Mie resonances in the wavelength range of interest, which offers an important perspective on the contribution of the optical magnetism in the proposed SPP couplers.

To better understand the coupling mechanism behind the observed SPP generation, calculated magnetic field ($|H|$) distributions corresponding to the two single-resonator systems at the resonance wavelengths (1418 and 1608 nm) are shown in Figs. 4(e) and 4(f), respectively. A significantly enhanced magnetic field is found at the Si-gold interface within the resonator, indicating the presence of strongly confined fields due to the interference-enhanced Mie resonance. Moreover, arising from the induced circular displacement current, the magnetic Mie resonance naturally leads to an antiparallel E_z distribution at the two opposite sides of the cuboid, enabling SPP generation along the $\pm y$ directions with a π phase difference. Figure 4(g) presents the at-resonance electric field distribution [$\mathrm{Re}(E_z)$] of the Cuboid A coupling system in a plane 10 nm above the gold substrate, while that of the Cuboid B case is shown in Fig. 4(h). Clearly, SP waves primarily propagating along the $\pm y$ directions are generated in both systems with a similar coupling efficiency, suggesting that a meta-optical system consisting of a pair of cuboids may be used to generate directional SPPs in a highly efficient manner.

Figure 5(a) shows the schematic of a directional coupler for SPPs based on the property of enhanced Mie resonance. Two Si cuboids with distinct dimensions (Cuboid A and Cuboid B) are used to break the symmetry and achieve directional generation of SPPs for normal incidence. Besides the intrinsic Mie resonance characteristics of each resonator, the relative distance (Dis) between the two cuboids has significant influence on the directional excitation of SP waves. The underlying mechanism involves two main factors: (1) the mutual coupling between the two resonators, especially when they are close to each other, and (2) the interference between the SPPs generated by each cuboid. The latter mechanism has been proposed to explain the directional SPP excitation in nano-slit systems [45]. To analyze

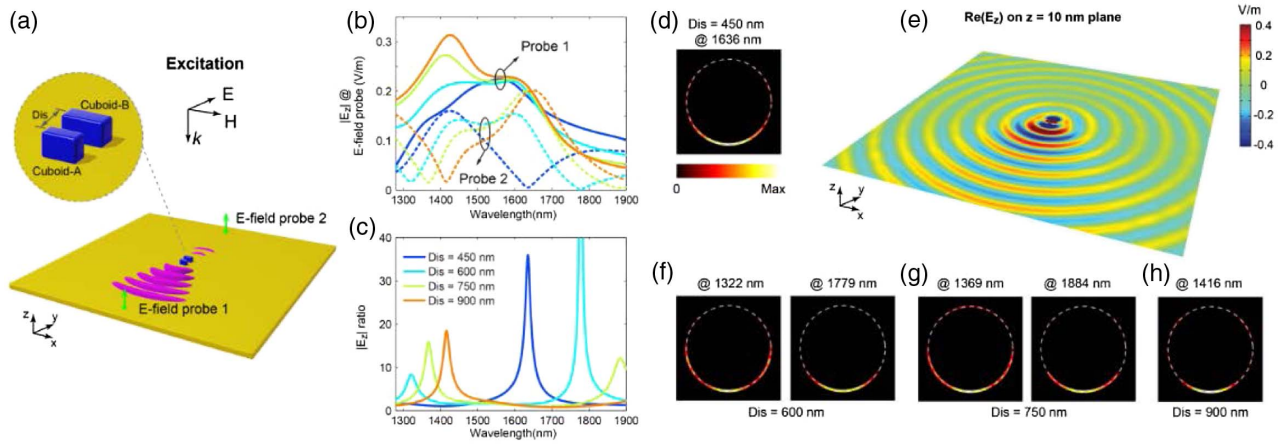

Fig. 5. Directional excitation of SPPs using a pair of high-index resonators. (a) Schematic of the meta-optical system for directional generation of SPPs. A y-polarized plane wave normally illuminates the resonators from the top. To monitor the excited SP waves, two electric field probes are placed 10 nm above the gold surface at $y = -5$ and $+5$ μm, respectively. (b) $|E_z|$ detected at the two E-field probes and, (c) the corresponding ratio between $|E_z|$ at the two probes ($|E_z|_{\text{probe1}}/|E_z|_{\text{probe2}}$), when the two cuboids are separated by a series of distances (Dis). (d) $|E_z|^2$ distribution on an imaginary circle (with a radius of 10 μm) at a wavelength of 1636 nm when Dis = 450 nm and (e) the corresponding electric field distribution of SPPs excited on the gold surface. (f)–(h) $|E_z|^2$ distributions corresponding to the $|E_z|$ ratio peaks in (c) on the imaginary circle.

the SPPs excited at the air–gold interface, two electric field probes (Probe 1 and Probe 2) are placed at a distance 5.0 μm away from the geometric center of the cuboid pair. Figure 5(b) shows the magnitude of $|E_z|$ detected at the two probes for a series of Dis values. In the wavelength range of interest, the SPPs detected at Probe 1 (solid curves) in general have greater amplitude than those detected at Probe 2 (dashed curves). A close inspection reveals that the plots corresponding to Probe 2 show one or two near-zero minimum values at certain wavelengths, where $|E_z|$ at Probe 1 has a reasonably high value. To better quantify the directionality of the generated SPPs, the ratio between the values of $|E_z|$ at Probe 1 and Probe 2 is illustrated in Fig. 5(c). The $|E_z|$ ratio provides an unambiguous measure of the directional excitation of SPPs at the air–gold interface, including the directionality and dispersion achieved by the proposed systems. When Dis = 450 nm, a more than 30 times contrast in terms of $|E_z|$ between SPP propagation along the $-y$ and $+y$ directions can be observed. The observed directional excitation of SP waves originates from the enhanced magnetic resonance in the Si resonators (Fig. 4), which enables this effect to occur over a relatively broad wavelength range. For instance, using an $|E_z|$ ratio of 5 as a measure, the coupler with Dis of 450 nm enables directional SPP excitation in a wavelength range from 1585 to 1677 nm. Furthermore, Fig. 5(c) also clearly reveals that the wavelength of the directional excitation of SPPs can be achieved by varying Dis, indicating the flexibility of the proposed meta-optical system for customized directional SPP couplers. This again verifies that the observed directional excitation of SP waves is primarily determined by the interference between the SPPs excited by both resonators. Accordingly, the pronounced $|E_z|$ ratio occurs at the wavelengths where constructive and deconstructive interference dominates the excitation of SPP waves propagating in the $-y$ and $+y$ direction, respectively.

It is of great importance to examine the propagation of the excited SPPs in the 2D (x–y) plane. Leakage radiation microscopy and conoscopic detection were previously used to experimentally observe the directional excitation of SPPs at an air–gold interface [48]. Here, by evaluating $|E_z|^2$, which is proportional to the power of the excited SPPs on an imaginary circle (centered at the geometric center of the cuboid pair and of radius of 10 μm), we obtain a more complete picture of the directional excitation of SPPs in the meta-optical system. Figure 5(d) shows the values obtained for $|E_z|^2$ on the imaginary circle at a wavelength of 1636 nm, corresponding to the $|E_z|$ ratio peak in Fig. 5(c) for the case of Dis = 450 nm. Although the power distribution diverges on the lower half circle, the components propagating primarily in the $-y$ direction carry most of the power. In sharp contrast, almost no power is delivered to the upper half circle. As illustrated in Fig. 5(e), the directional propagation of an SPP wave is made more evident from the electric field distribution [Re(E_z)] on a plane 10 nm above the gold substrate. Figures 5(f)–5(h) show the $|E_z|^2$ evaluation results for other values of Dis at the peak wavelength(s) of the $|E_z|$ ratio in Fig. 5(c). For the case of Dis = 600 nm [Fig. 5(f)], the SPPs excited at a shorter wavelength (e.g., 1322 nm) are more divergent compared with those at a longer wavelength (e.g., 1779 nm). A similar observation can be made regarding Fig. 5(g) for the case of Dis = 750 nm. This can be attributed to the fact that the Si cuboid pair is relatively larger compared with the periodicity of the SPPs excited at the shorter wavelengths, which, accordingly, enhances the in-plane diffraction effects. Nevertheless, it can be seen that, in all cases, most of the power of the excited SPPs is located on the lower half of the imaginary circle, indicating that meta-optics-based systems are an effective platform for directional excitation of SPPs.

5. DISCUSSION

It should be noted that the three processes, i.e., TPA, free carrier generation, and the lattice heating effect that determine the transient response of Si nanostructures, have distinct transient

characteristics. Particularly, the TPA is the fastest process of the three, while the intrinsic carrier relaxation in a-Si:H is primarily determined by the first-order trap-assisted process [43] and the second-order bimolecular recombination rate [38]. The lattice heating, which causes a thermo-optic effect, is generally the slowest process and determines the falling time constant of the nonlinear modulation. Accordingly, high-speed modulation windows might be achieved through further optimization of both the Si meta-atoms (such as the geometrical parameters and their alignment) and the pump pulses (including the wavelength, polarization, intensity, etc.) [38,39].

Besides enabling transient intensity tuning, dielectric resonators have also been used to realize high-speed wavefront manipulation based on reflection phase modulation at frequencies of ~10 kHz [49]. In the nonlinear regime, selective excitations of electric and magnetic resonances in dielectric nanostructures have recently been exploited for a variety of optical nonlinearities [50–53]. Given the intriguing role that the magnetic response plays in these studies, we envision that further tailoring of the optical magnetism in high-index resonators through interference engineering can provide more degrees of freedom in the design of metasurfaces with customized nonlinearity.

Although here we have limited our discussion mainly to meta-optics-based systems that operate in the reflection mode, the interference-enhanced magnetic Mie resonance can also be explored for effective operation in the transmission mode. This can be implemented by using a Bragg mirror whose reflection and transmission bands can be custom-designed. Bragg mirror-based meta-optical systems are expected to be particularly suitable for nonlinear generation. In particular, the metasurface can be designed to enable interference-enhanced optical response at fundamental wavelengths, while its influence on the resultant enhanced harmonic generation (e.g., SHG, THG) can be engineered independently. Given the fact that the reflection behavior of the Ge resonator arrays at visible frequencies primarily depends on the electric and magnetic dipole modes, we envision that the use of interference-enhanced magnetism may provide a pathway to achieving better color intensities.

6. CONCLUSION

In this work, we have revealed that optical magnetism in high-index resonators can be significantly enhanced by adding a back mirror to the system, with a concomitant increase in field confinement and enhancement. To highlight the transformative advancements offered by the proposed mechanism in tailoring the response of meta-optical systems, we present two proof-of-concept demonstrations. In particular, using a theoretical model to mimic the optical pump–probe experiments, we study the ultrafast tuning of a Si nanodisk array on a gold ground plane. Due to the critical coupling effect, more than an order of magnitude stronger optical response modulation was observed around the guided resonance wavelength in the near-IR region, when the pump fluence is 10% of that used in previous studies. This superior ultrafast tuning behavior originates from the interference-enhanced magnetic Mie resonance of the Si nanodisk resonators. Furthermore, by exploiting the Mie resonance of individual Si resonators located on top of a gold film, we show that a pair of Si cuboids can serve as magnetic antennas for directional excitation of SPPs. The capability of controlling both magnitude and phase of the excited SPPs makes the high-index resonators a promising candidate for a subwavelength and efficient SPP source, which is highly desired in potential integrated plasmonic systems. Given the increasing interest in man-made optical magnetism, we envision that exploitation of the proposed interference-enhanced magnetic Mie resonance phenomenon will promote the development of meta-optics in the linear and nonlinear regimes.

Funding. National Science Foundation (NSF DMR-1420620).

†These authors contributed equally to this work.

REFERENCES

1. V. M. Shalaev, "Optical negative-index metamaterials," Nat. Photonics **1**, 41–48 (2007).
2. C. M. Soukoulis and M. Wegener, "Past achievements and future challenges in the development of three-dimensional photonic metamaterials," Nat. Photonics **5**, 523–530 (2011).
3. J. B. Pendry, A. J. Holden, D. J. Robbins, and W. J. Stewart, "Magnetism from conductors and enhanced nonlinear phenomena," IEEE Trans. Microw. Theory Tech. **47**, 2075–2084 (1999).
4. D. Schurig, J. J. Mock, B. J. Justice, S. A. Cummer, J. B. Pendry, A. F. Starr, and D. R. Smith, "Metamaterial electromagnetic cloak at microwave frequencies," Science **314**, 977–980 (2006).
5. M. W. Klein, C. Enkrich, M. Wegener, and S. Linden, "Second-harmonic generation from magnetic metamaterials," Science **313**, 502–504 (2006).
6. J. K. Gansel, M. Thiel, M. S. Rill, M. Decker, K. Bade, V. Saile, G. von Freymann, S. Linden, and M. Wegener, "Gold helix photonic metamaterial as broadband circular polarizer," Science **325**, 1513–1515 (2009).
7. J. B. Pendry, "Negative refraction makes a perfect lens," Phys. Rev. Lett. **85**, 3966–3969 (2000).
8. D. R. Smith, W. J. Padilla, D. C. Vier, S. C. Nemat-Nasser, and S. Schultz, "Composite medium with simultaneously negative permeability and permittivity," Phys. Rev. Lett. **84**, 4184–4187 (2000).
9. T. J. Yen, W. J. Padilla, N. Fang, D. C. Vier, D. R. Smith, J. B. Pendry, D. N. Basov, and X. Zhang, "Terahertz magnetic response from artificial materials," Science **303**, 1494–1496 (2004).
10. Q. Zhao, J. Zhou, F. Zhang, and D. Lippens, "Mie resonance-based dielectric metamaterials," Mater. Today **12**, 60–69 (2009).
11. Q. Zhao, L. Kang, B. Du, H. Zhao, Q. Xie, X. Huang, B. Li, J. Zhou, and L. Li, "Experimental demonstration of isotropic negative permeability in a three-dimensional dielectric composite," Phys. Rev. Lett. **101**, 027402 (2008).
12. H.-T. Chen, A. J. Taylor, and N. Yu, "A review of metasurfaces: physics and applications," Rep. Prog. Phys. **79**, 076401 (2016).
13. X. Luo, "Principles of electromagnetic waves in metasurfaces," Sci. China Phys. Mech. Astron. **58**, 594201 (2015).
14. A. I. Kuznetsov, A. E. Miroshnichenko, M. L. Brongersma, Y. S. Kivshar, and B. Luk'yanchuk, "Optically resonant dielectric nanostructures," Science **354**, aag2472 (2016).
15. S. Kruk and Y. Kivshar, "Functional meta-optics and nanophotonics governed by Mie resonances," ACS Photon. **4**, 2638–2649 (2017).
16. Y. Kivshar, "All-dielectric meta-optics and non-linear nanophotonics," Natl. Sci. Rev. **5**, 144–158 (2018).
17. Q. Zhao, Z. Xiao, F. Zhang, J. Ma, M. Qiao, Y. Meng, C. Lan, B. Li, J. Zhou, P. Zhang, N.-H. Shen, T. Koschny, and C. M. Soukoulis, "Tailorable zero-phase delay of subwavelength particles toward miniaturized wave manipulation devices," Adv. Mater. **27**, 6187–6194 (2015).

18. Y. H. Fu, A. I. Kuznetsov, A. E. Miroshnichenko, Y. F. Yu, and B. Luk'yanchuk, "Directional visible light scattering by silicon nanoparticles," Nat. Commun. **4**, 1527 (2013).
19. S. Person, M. Jain, Z. Lapin, J. J. Sáenz, G. Wicks, and L. Novotny, "Demonstration of zero optical backscattering from single nanoparticles," Nano Lett. **13**, 1806–1809 (2013).
20. I. Staude, A. E. Miroshnichenko, M. Decker, N. T. Fofang, S. Liu, E. Gonzales, J. Dominguez, T. S. Luk, D. N. Neshev, I. Brener, and Y. Kivshar, "Tailoring directional scattering through magnetic and electric resonances in subwavelength silicon nanodisks," ACS Nano **7**, 7824–7832 (2013).
21. X. Luo, D. Tsai, M. Gu, and M. Hong, "Subwavelength interference of light on structured surfaces," Adv. Opt. Photon. **10**, 757–842 (2018).
22. S. Fan and J. D. Joannopoulos, "Analysis of guided resonances in photonic crystal slabs," Phys. Rev. B **65**, 235112 (2002).
23. C. W. Hsu, B. Zhen, J. Lee, S.-L. Chua, S. G. Johnson, J. D. Joannopoulos, and M. Soljačić, "Observation of trapped light within the radiation continuum," Nature **499**, 188–191 (2013).
24. H. Yang, D. Zhao, S. Chuwongin, J.-H. Seo, W. Yang, Y. Shuai, J. Berggren, M. Hammar, Z. Ma, and W. Zhou, "Transfer-printed stacked nanomembrane lasers on silicon," Nat. Photonics **6**, 615–620 (2012).
25. J. R. Piper and S. Fan, "Total absorption in a graphene monolayer in the optical regime by critical coupling with a photonic crystal guided resonance," ACS Photon. **1**, 347–353 (2014).
26. N. Liu, M. Mesch, T. Weiss, M. Hentschel, and H. Giessen, "Infrared perfect absorber and its application as plasmonic sensor," Nano Lett. **10**, 2342–2348 (2010).
27. L. Kang, S. P. Rodrigues, M. Taghinejad, S. Lan, K.-T. Lee, Y. Liu, D. H. Werner, A. Urbas, and W. Cai, "Preserving spin states upon reflection: linear and nonlinear responses of a chiral meta-mirror," Nano Lett. **17**, 7102–7109 (2017).
28. L. Kang, Y. Cui, S. Lan, S. P. Rodrigues, M. L. Brongersma, and W. Cai, "Electrifying photonic metamaterials for tunable nonlinear optics," Nat. Commun. **5**, 4680 (2014).
29. L. Liu, L. Kang, T. S. Mayer, and D. H. Werner, "Hybrid metamaterials for electrically triggered multifunctional control," Nat. Commun. **7**, 13236 (2016).
30. H. Sugimoto and M. Fujii, "Broadband dielectric-metal hybrid nanoantenna: silicon nanoparticle on a mirror," ACS Photon. **5**, 1986–1993 (2018).
31. F. Deng, H. Liu, and S. Lan, "Metal substrate-induced line width compression in the magnetic dipole resonance of a silicon nanosphere illuminated by a focused azimuthally polarized beam," Nanoscale Res. Lett. **13**, 395 (2018).
32. F. Di Mei, L. Falsi, M. Flammini, D. Pierangeli, P. Di Porto, A. J. Agranat, and E. DelRe, "Giant broadband refraction in the visible in a ferroelectric perovskite," Nat. Photonics **12**, 734–738 (2018).
33. M. Esfandyarpour, E. C. Garnett, Y. Cui, M. D. McGehee, and M. L. Brongersma, "Metamaterial mirrors in optoelectronic devices," Nat. Nanotechnol. **9**, 542–547 (2014).
34. S. Liu, M. B. Sinclair, T. S. Mahony, Y. C. Jun, S. Campione, J. Ginn, D. A. Bender, J. R. Wendt, J. F. Ihlefeld, P. G. Clem, J. B. Wright, and I. Brener, "Optical magnetic mirrors without metals," Optica **1**, 250–256 (2014).
35. Z. Ma, S. M. Hanham, P. Albella, B. Ng, H. T. Lu, Y. Gong, S. A. Maier, and M. Hong, "Terahertz all-dielectric magnetic mirror metasurfaces," ACS Photon. **3**, 1010–1018 (2016).
36. X. Liu, Q. Zhao, C. Lan, and J. Zhou, "Isotropic Mie resonance-based metamaterial perfect absorber," Appl. Phys. Lett. **103**, 031910 (2013).
37. Y. Cui, K. H. Fung, J. Xu, H. Ma, Y. Jin, S. He, and N. X. Fang, "Ultrabroadband light absorption by a sawtooth anisotropic metamaterial slab," Nano Lett. **12**, 1443–1447 (2012).
38. G. Della Valle, B. Hopkins, L. Ganzer, T. Stoll, M. Rahmani, S. Longhi, Y. S. Kivshar, C. De Angelis, D. N. Neshev, and G. Cerullo, "Nonlinear anisotropic dielectric metasurfaces for ultrafast nanophotonics," ACS Photon. **4**, 2129–2136 (2017).
39. M. R. Shcherbakov, P. P. Vabishchevich, A. S. Shorokhov, K. E. Chong, D.-Y. Choi, I. Staude, A. E. Miroshnichenko, D. N. Neshev, A. A. Fedyanin, and Y. S. Kivshar, "Ultrafast all-optical switching with magnetic resonances in nonlinear dielectric nanostructures," Nano Lett. **15**, 6985–6990 (2015).
40. Y. Yang, I. I. Kravchenko, D. P. Briggs, and J. Valentine, "All-dielectric metasurface analogue of electromagnetically induced transparency," Nat. Commun. **5**, 5753 (2014).
41. Y. Yang, W. Wang, A. Boulesbaa, I. I. Kravchenko, D. P. Briggs, A. Puretzky, D. Geohegan, and J. Valentine, "Nonlinear Fano-resonant dielectric metasurfaces," Nano Lett. **15**, 7388–7393 (2015).
42. M. Rahmani, L. Xu, A. E. Miroshnichenko, A. Komar, R. Camacho-Morales, H. Chen, Y. Zárate, S. Kruk, G. Zhang, D. N. Neshev, and Y. S. Kivshar, "Reversible thermal tuning of all-dielectric metasurfaces," Adv. Funct. Mater. **27**, 1700580 (2017).
43. D. G. Baranov, S. V. Makarov, V. A. Milichko, S. I. Kudryashov, A. E. Krasnok, and P. A. Belov, "Nonlinear transient dynamics of photoexcited resonant silicon nanostructures," ACS Photon. **3**, 1546–1551 (2016).
44. P. Lalanne, J. P. Hugonin, and J. C. Rodier, "Theory of surface plasmon generation at nanoslit apertures," Phys. Rev. Lett. **95**, 263902 (2005).
45. F. López-Tejeira, S. G. Rodrigo, L. Martín-Moreno, F. J. García-Vidal, E. Devaux, T. W. Ebbesen, J. R. Krenn, I. P. Radko, S. I. Bozhevolnyi, M. U. González, J. C. Weeber, and A. Dereux, "Efficient unidirectional nanoslit couplers for surface plasmons," Nat. Phys. **3**, 324–328 (2007).
46. J. Chen, Z. Li, S. Yue, and Q. Gong, "Highly efficient all-optical control of surface-plasmon-polariton generation based on a compact asymmetric single slit," Nano Lett. **11**, 2933–2937 (2011).
47. A. Pors, M. G. Nielsen, T. Bernardin, J.-C. Weeber, and S. I. Bozhevolnyi, "Efficient unidirectional polarization-controlled excitation of surface plasmon polaritons," Light Sci. Appl. **3**, e197 (2014).
48. Y. Liu, S. Palomba, Y. Park, T. Zentgraf, X. Yin, and X. Zhang, "Compact magnetic antennas for directional excitation of surface plasmons," Nano Lett. **12**, 4853–4858 (2012).
49. Y. Horie, A. Arbabi, E. Arbabi, S. M. Kamali, and A. Faraon, "High-speed, phase-dominant spatial light modulation with silicon-based active resonant antennas," ACS Photon. **5**, 1711–1717 (2018).
50. S. V. Makarov, M. I. Petrov, U. Zywietz, V. Milichko, D. Zuev, N. Lopanitsyna, A. Kuksin, I. Mukhin, G. Zograf, E. Ubyivovk, D. A. Smirnova, S. Starikov, B. N. Chichkov, and Y. S. Kivshar, "Efficient second-harmonic generation in nanocrystalline silicon nanoparticles," Nano Lett. **17**, 3047–3053 (2017).
51. S. Chen, M. Rahmani, K. F. Li, A. Miroshnichenko, T. Zentgraf, G. Li, D. Neshev, and S. Zhang, "Third harmonic generation enhanced by multipolar interference in complementary silicon metasurfaces," ACS Photon. **5**, 1671–1675 (2018).
52. S. T. Ha, Y. H. Fu, N. K. Emani, Z. Pan, R. M. Bakker, R. Paniagua-Domínguez, and A. I. Kuznetsov, "Directional lasing in resonant semiconductor nanoantenna arrays," Nat. Nanotechnol. **13**, 1042–1047 (2018).
53. L. Wang, S. Kruk, K. Koshelev, I. Kravchenko, B. Luther-Davies, and Y. Kivshar, "Nonlinear wavefront control with all-dielectric metasurfaces," Nano Lett. **18**, 3978–3984 (2018).